Magnetic-field-dependent surface resistance and two-level critical-state model for granular superconductors

L. Ji,* M. S. Rzchowski, N. Anand, and M. Tinkham
Department of Physics and Division of Applied Sciences, Harvard University, Cambridge, Massachusetts 02138
(Received 5 May 1992; revised manuscript received 5 August 1992)

We develop a two-level critical-state model for calculating the intergranular fluxon density of a granular superconductor as a function of the external magnetic field, and compare it to our measurements of magnetic-field hysteresis of the microwave surface resistance of $YBa_2Cu_3O_7$ bulk samples and of Nb-Cu-Nb proximity-effect Josephson-junction arrays. Our model deals with the magnetic-flux profiles on both macroscopic and local levels, as the intergranular critical current density is significantly smaller than the intragranular critical current density. We first solve the simplified special case of an infinitely large flat-slab geometry with an ideal ordered superconducting lattice microstructure, where the resulting intergranular fluxon density leads to anomalous magnetic hysteresis as observed experimentally. Then we generalize to disordered samples by introducing a type of clusters of grains. In this case, fluxons move freely in and out of the sample through percolative paths between the clusters, forming a structure topologically identical to our simplified ordered structure. The sizes of clusters depend on the microstructure and the stiffness of flux-line lattices, and on whether the sample is cooled in zero magnetic field or in a magnetic field. These dependences are studied both theoretically and experimentally. Finally, we use the model to explain features observed in transport critical-current and flux-creep measurements.

I. INTRODUCTION

Microwave-loss measurements have been used extensively to study high-temperature superconductors. When an external dc magnetic field is applied, a variety of different behaviors have been reported.[1-5] Some observed magnetic-field dependences of the surface resistance seem to be contrary to the case for the conventional superconductors. For example, we reported earlier[4] that the surface resistance of a zero-field-cooled (ZFC) sample is higher (instead of lower, as in the conventional case) than that of a field-cooled (FC) sample, which was accounted for by the granular structure of the sample. In this paper, we extend the idea that the magnetic-field-dependent microwave loss in granular materials is influenced by the granular structure, and give a more quantitative study of the magnetic-field hysteresis, history dependence, and time dependence of the surface resistance.[6]

First, let us consider the microwave loss of a conventional homogeneous superconductor in an external dc magnetic field. In the mixed state of a type-II superconductor, magnetic flux penetrates in the form of flux tubes called fluxons, each carrying a quantum of flux $\Phi_0 = hc/2e$. Under an rf field, the motion of fluxons is governed by their viscous drag and the restoring force from pinning centers. Here we discuss the so-called perpendicular mode where the rf current induced in the sample is perpendicular to the external dc magnetic field and the fluxons. Gittleman and Rosenblum[7] have shown that at sufficiently high frequencies, viscous drag dominates, and fluxons oscillate about their equilibrium positions, dissipating energy as though they were unpinned. In this high-frequency region, similar to the Bardeen-Stephen flux-flow model,[8] the sample dissipates energy in proportion to the number of fluxons it contains, and inversely proportional to the coefficient of viscous drag. Specifically, the flux-flow resistivity is given by

$$\rho_B = \rho_n \frac{B}{H_{c2}} = \frac{\Phi_0 B}{c^2 \eta} = \frac{n \Phi_0^2}{c^2 \eta} , \tag{1}$$

where $n = B/\Phi_0$ is the fluxon number density, η is the coefficient of the viscous drag, ρ_n is the normal-state resistivity, and H_{c2} is the upper critical field. In the microwave-flux-flow experiments done by Gittleman and Rosenblum and later by others, thin films were placed in a perpendicular dc magnetic field; therefore $B = H$, and no magnetic hysteresis was observed. However, Eq. (1) should remain valid for samples with a different geometry, which would show a magnetic hysteresis. For the general case of a spatially dependent flux density in the sample, and if we also assume the rf skin depth is smaller than the sample thickness, Eq. (1) can be modified as[6]

$$R_s = R_n \sqrt{\langle |h| \rangle / H_{c2}} , \tag{2}$$

where R_s and R_n are the surface resistances in the superconducting and normal state, respectively, $h(x,y)$ is the local flux density, which depends on spatial coordinates x and y, and $\langle |h| \rangle$ is a spatial average of the absolute value of the flux density h. Note that $\langle |h| \rangle \neq B = \langle h \rangle$, the averaged flux density of the sample, which is the quantity measured by magnetization measurements.

Using the critical-state model,[9,10] $h(x,y)$, and therefore $\langle h \rangle$ and $\langle |h| \rangle$, can be calculated as a function of the external field $H_{\rm ext}$. However, the analytical solution for the critical-state model is available only for a limited

number of special cases (e.g., Refs. 9–13). In Appendix A, we have calculated the formulas for a long slab in a parallel dc magnetic field, with a simplified Kim-Anderson model in which $J_c(x,y) \sim 1/h(x,y)$, where x,y are again spatial coordinates. Figures 1(a) and 1(b) are the initial and hysteresis curves of the flux density $B = \langle h \rangle$, and the surface resistance R_s using Eq. (2), calculated for an external dc field cycled between $\pm H^*$, where H^* is the penetration field of the sample. Two features are clearly shown in Fig. 1: (1) for the same value of H_{ext}, both the averaged flux density B and the surface resistance R_s in the decreasing H_{ext} curve are higher than that in the increasing H_{ext} curve, resulting from the trapped fluxons; (2) in decreasing H_{ext}, the minimum of R_s is obtained at a negative value of H_{ext}, where $B = 0$. Note that the exact solution we used here is calculated only for the special case of a long cylinder, which is unusual for microwave measurements. The actual shape of the hysteresis loops depends on the maximum field applied, the geometry of the sample, and the actual field dependence of critical current density. However, the above two features of the magnetic hysteresis are rather general for any homogeneous sample (regardless of their actual geometries), as they are simply based on flux trapping. Such features have been seen in conventional superconductors such as Nb samples, which we discuss later, and in high-T_c samples[1,5] at low temperature and small dc fields. However, the surface resistance measurement on "single crystals" at high temperature and/or high fields, and ceramic samples generally, have shown the opposite results, as reported by many groups.[2,5,6] Figure 2 shows a typical experimental result we measured on ceramic samples, where the surface resistance R_s in the decreasing H_{ext} curve is lower than that in the increasing H_{ext} curve, and the minimum of R_s is obtained before H_{ext} reaches zero. The details of the sample preparation and the measurement apparatus will be reported in a later section.

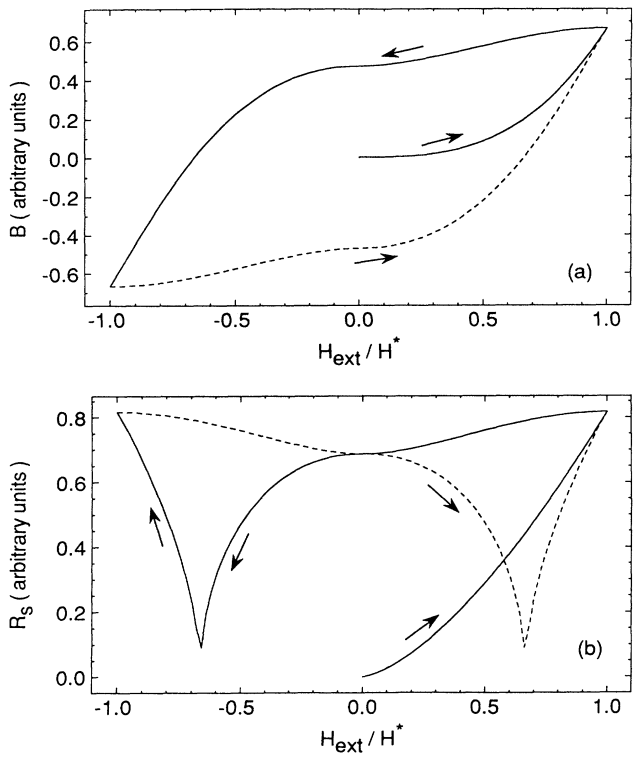

FIG. 1. The case of homogeneous superconductors. Initial curves and hysteresis curves predicted by Kim-Anderson critical-state model: (a) the averaged flux density B, (b) the surface resistance R_s. The arrows indicate the direction of the change of the external magnetic field.

To understand this anomalous magnetic hysteresis observed in granular samples, one must first clarify the difference between a homogeneous sample and a granular sample. For a homogeneous sample, all fluxons in it contribute to the microwave loss with the same weight. For granular superconductors, since the viscosity for fluxons between the grains is orders of magnitude smaller than that for fluxons in the grains, the microwave loss is mainly due to the flux-flow-like dissipation of intergranular fluxons.[14] In the regime where the flow-flow-like dissipation process dominates the loss,[4]

$$R_s = \sqrt{2\pi\omega\Phi_0^2 n_j/c^4\eta_j}\ , \tag{3}$$

where n_j is the intergranular fluxon number density, η_j is the coefficient of the viscous drag in the intergranular regions, and ω is the angular frequency. Here the surface resistance is proportional to $n_j^{1/2}$, the square root of the intergranular fluxon density. Thus the measurement of the magnetic-field-dependent microwave surface resistance will enable us to study the motion of intergranular fluxons.

Electromagnetic properties in high-T_c superconductors are strongly influenced by its granularity.[15,16] In this paper, we develop a two-level critical-state model for the calculation of the intergranular fluxon density of a granular superconductor as a function of the external magnetic field and its history, and compare it to our measurements of magnetic-field hysteresis of the microwave surface resistance of bulk samples of $YBa_2Cu_3O_7$ and of Nb-Cu-Nb proximity-effect Josephson-junction arrays. The

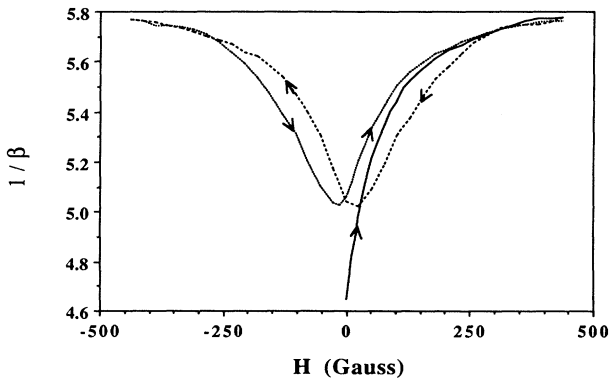

Fig. 2. Surface resistance change $1/\beta$ vs external magnetic field measured on a ZFC $YBa_2Cu_3O_7$ bulk sample at 78 K. The arrows indicate the direction of the change of the external magnetic field.

two-level model we propose deals with the flux profiles on both macroscopic and local levels. The basic ideas of the two-level critical-state model are discussed in Sec. II. In Sec. III, we simplify the general problem and solve it for the special case of an infinitely large flat-slab geometry and for an ideal ordered superconducting lattice microstructure. We calculate the intergranular fluxon density as a function of the external magnetic field, which gives the underlying mechanism of the anomalous hysteresis observed. Then, in Sec. IV, we extend our results to disordered systems. For granular samples with random microstructures, we propose that some fluxons can bend around the superconducting grains and stay unpinned. These fluxons move freely in and out of the sample through percolative paths between the clusters of grains, similar to the picture proposed by Gurevich.[17] The cluster structure is topologically similar to the structure we solve in Sec. III and therefore our results can be extended to an arbitrary granular system. For ZFC samples, the size of the clusters depends on the maximum field applied. For FC samples, the cluster size is much larger and almost independent of the applied field. Section V reports the microwave surface resistance measurements of bulk $YBa_2Cu_3O_7$ samples and Nb-Cu-Nb proximity-effect Josephson-junction arrays. The results will be compared to the two-level critical-state model. In Sec. VI, we use the model to account for features observed in the transport critical current and the flux-creep measurements. Section VII is a conclusion. Some formulas used in the calculation of critical-state quantities are listed in the Appendixes.

II. BASIC CONCEPTS OF THE TWO-LEVEL CRITICAL-STATE MODEL

The conventional critical-state model deals with macroscopically homogeneous samples, where a single critical current density controls the gradient of flux density everywhere. For granular materials, however, two distinct critical current densities exist: a large critical current density J_{cg} inside the grains, and a much weaker one J_{cJ} reflecting the intergranular Josephson coupling. Thus the gradient of the flux density in the grains can be much larger than that in the boundaries between the grains. For this reason, we propose that the critical-state model in a granular system should be built on two levels. On the macroscopic level, the flux density averaged over a scale of many grains should have a gradient determined by the macroscopically flowing intergranular critical current density J_{cJ}. On the local level within single grains, a critical state is established with a flux density gradient determined by the intragranular critical current density J_{cg}. The flux density in the grain boundaries influences this local critical state by supplying the effective external field. On both levels, the relation between the shape of the flux profiles and the outside field is determined according to the principles of the original critical-state model.[9] We give a schematic representation in Fig. 3, where the dashed line is the averaged flux profile on the macroscopic level and the solid line is the flux profile on the local level.

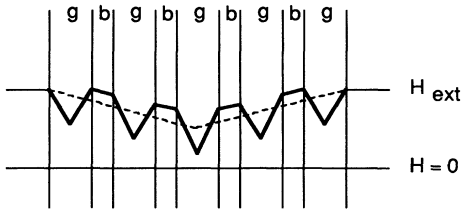

FIG. 3. A figurative representation of the flux profile in a granular sample where grains (denoted as g regions) and grain boundaries (denoted as b regions) have different flux density gradient. The solid line represents the critical states on the local level and the dashed line represents the critical state on the macroscopic level.

Though we explicitly assumed two distinct levels in the above paragraph, the same principle applies for any system with different levels of pinning strength, whether it is two levels or more. For example, some grains can form strongly Josephson-coupled clusters, and making a new level where the critical current density within it is much larger than that for the whole sample but smaller than that for the grains. However, we will limit our discussion to the two-level case and try to explain some experimental results using it, though a real sample may contain many more levels.

If the macroscopic screening is dominant, we expect that a two-level critical-state system will still show behaviors similar to that of a homogeneous sample as shown in Fig. 1. However, when the local critical state becomes dominant, a dramatically different picture will appear. Figure 2 shows anomalous hysteresis curves measured on a granular $YBa_2Cu_3O_7$ bulk sample, which we will attribute to such a case.

III. FLUXONS IN AN ORDERED SUPERCONDUCTING LATTICE

The general problem of an arbitrary granular sample with finite sizes is difficult to solve.[18] However, the case of an infinitely large flat slab (also composed of an ordered structure) in a perpendicular magnetic field is solvable analytically, and contains the physics we wish to explore. As shown in Fig. 4, we assume the thickness of the slab is d, and the microscopic composition of this flat slab is an ordered lattice of superconducting cubes (or grains), where a is the lattice constant and L_g is the side of the superconducting cubes. We further assume $L_g \sim a$, so that the grain boundary region is small compared to the grains, and that $d \gg a$, which makes the critical-state model on the local level easier, as we will discuss later.

We define two types of fluxons according to their dc pinning characteristics: (1) *grain-pinned fluxons,* denoted by h_p, are those *pinned* by pinning centers within the grains; (2) *grain-boundary fluxons,* denoted by h_f, are those that never pass through grains; they are relatively *free,* since they are not pinned by the strong pinning centers in the grains. Throughout this paper, we use h as the microscopic magnetic flux density, with h_p for the pinned region of the local critical state, and h_f for the re-

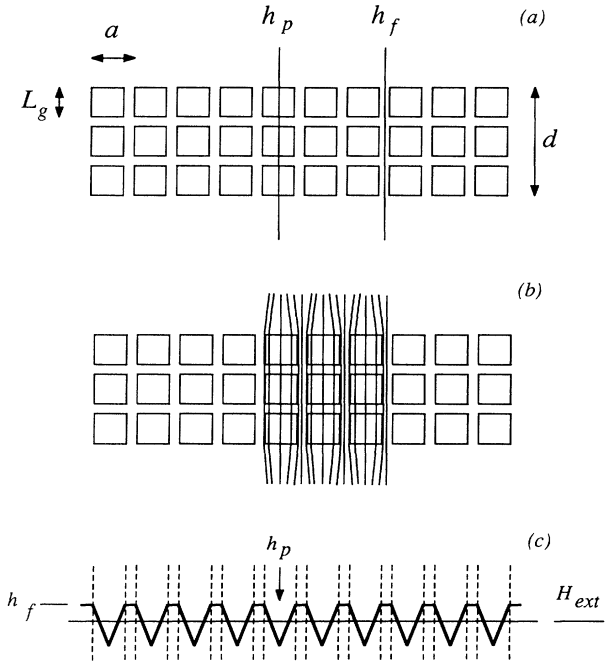

FIG. 4. (a) Side view of a flat slab composed of an ordered lattice of superconducting cubes in a perpendicular field. Examples of the *grain-pinned fluxons* (the line with h_p) and the *grain-boundary fluxons* (the line with h_f) are also shown. (b) A figurative representation of the flux lines in critical state. (c) The flux profile in critical state.

gion where free grain-boundary fluxons exist. Figure 4 shows the two kinds of fluxons and the two-level critical-state flux profile.

Due to the macroscopic spatial uniformity, the grain-boundary-flux density h_f is a constant, as shown in Fig. 4(c), if the intergranular critical current density is negligible compared to the intragranular critical current density. The grain-pinned-flux density h_p varies within grains, and will be determined later according to the critical state on the local level. For our simplified system in a perpendicular magnetic field, the average flux density is equal to the external magnetic field, $H_{\rm ext}$, since the sample is infinite in horizontal directions. Therefore,

$$(1-s_p)h_f+s_p\langle h_p\rangle=H_{\rm ext}\ , \tag{4}$$

where s_p is the cross-sectional fraction of the pinned area (or the local critical-state region), and $\langle h_p\rangle$ is the averaged grain-pinned-flux density over it. For our simplified case, the cross-sectional area of the local critical-state region is L_g^2, the area of the weak boundary region is $(a^2-L_g^2)$, thus

$$s_p^{(0)}=\frac{L_g^2}{a^2}\ , \tag{5}$$

where we used superscript "(0)" to denote the simplified ordered case.

The total intergranular fluxon density n_j is

$$n_j=\frac{1}{\Phi_0}[(1-s_p)|h_f|+s_p x\langle|h_p|\rangle]\ , \tag{6}$$

where the parameter x in the ordered case is

$$x^{(0)}=\frac{a-L_g}{a}\ . \tag{7}$$

Here the first term in the bracket in Eq. (6) is due to the grain-boundary fluxons and the second term is due to the grain-pinned fluxons that pass through weak link regions between grains over a fraction $x^{(0)}=(a-L_g)/a$, of their length. Also, we have called n_j the intergranular *fluxon density* instead of *flux density,* since in microwave surface resistance study we measure the total number of the intergranular fluxons (regardless of their directions).

As a result of the assumed infinitely large flat-slab system, Eq. (4) serves as a key to simplify the complicated general problem discussed in the last section. Physically, assuming the sample to be an infinitely large flat slab is equivalent to saying that we can neglect the screening of the external field on the macroscopic level. It is preferable to compare this model to samples with the flat-slab geometry. However, because the intergranular critical current in high-temperature granular superconductors is very small, our results should be applicable to any cases where the macroscopic screening becomes negligible in a weak field.

A *grain-pinned fluxon* passes through a vertical row of superconducting cubes, as shown in Fig. 4. For our case of $L_g\sim a$ and of a perpendicular (vertical) external field, such a vertical row of superconducting cubes behaves like a solid rod of square shaped cross section L_g^2 and height d. To this superconducting rod, the effective external field is the flux density in the weak link region h_f. We can find the relation between h_p and h_f according to the critical-state model, and then we can easily obtain

$$\langle h_p\rangle=f(h_f)\ , \tag{8}$$

$$\langle|h_p|\rangle=g(h_f)\ . \tag{9}$$

Here $f(x)$ and $g(x)$ are given in Appendix B, calculated using Bean's critical-state model (which assumes a *constant* critical current density) for the case of an infinitely long slab of penetration field H^*. (The magnetic field is parallel to the plane of a *long* slab whereas it is perpendicular to the plane in the so-called *flat*-slab geometry.) Since the general features of the two-level critical state we discuss here do not depend on the specific critical-state model used for the grains, we choose the Bean model for its mathematical simplicity. We further approximate the long rod with a long slab for the simplicity of algebra: Such an approximation does not severely change the underlying physics. The penetration field H_g^* for each rod is

$$H_g^*\approx\frac{2\pi}{c}J_{cg}L_g\ . \tag{10}$$

Using Eqs. (4)–(10), one can theoretically solve for the intergranular fluxon density n_j as a function of the external field $H_{\rm ext}$. Only two parameters are needed, one is H_g^* of the grains, the other is L_g/a, which is related to the microstructure. Though h_f is not directly proportional to $H_{\rm ext}$, their relation is monotonic: (1) when $H_{\rm ext}$

increases, h_f increases; (2) when H_{ext} decreases, h_f decreases. Therefore, using Eqs. (4) and (6), we parametrically plot n_j vs H_{ext} with h_f as the free parameter. Figure 5 shows one such plot, where an external field H_{ext} is applied to a ZFC sample, rising from zero to $0.82H_g^*$ (which corresponds in this example to $h_f=H_g^*$), then decreasing to $-0.82H_g^*$, then increasing again to $0.82H_g^*$.

Contrary to the conventional case as shown in Fig. 1(b), Fig. 5 shows two significant *anomalous* features: (1) for the same value of H_{ext}, n_j in the decreasing H_{ext} curve is *lower* than that in the increasing H_{ext} curve; (2) the minimum of n_j is obtained before H_{ext} reaches zero in decreasing $|H_{ext}|$. These two features have been observed experimentally in granular samples, as shown earlier in Fig. 2. To help to understand the underlying physics, Fig. 6 shows the flux profiles (dark solid lines) and H_{ext} (dashed lines) for points A, B, C, and D of the decreasing H_{ext} curve in Fig. 5. Physically, as H_{ext} decreases from the maximum fields H_{max}, fluxons move out of the unpinned regions first, giving a lower n_j (the first anomaly). The minimum of n_j is reached at point B, where the unpinned fluxon density $h_f=0$, but the macroscopic averaged flux density B (equals to the external field H_{ext} in the infinitely flat-slab case here) is still positive (the second anomaly). The important point here is that n_j and B are two different physical quantities.

Now we discuss how H_m depends on H_{max}. Again we use h_f as a free parameter, and notice that H_m is reached when $h_f=0$. From Eq. (4), the corresponding external field H_m is equal to $s_p\langle|h_p|\rangle$. Using the results in Appendix B, we have

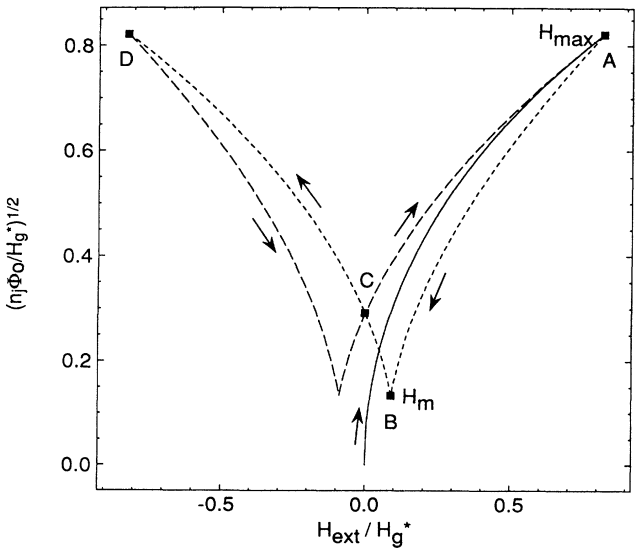

FIG. 5. The calculated (normalized) intergranular fluxon density $n_j^{1/2}$ vs the external field H_{ext} for an ordered ZFC sample with $L_g=0.8a$, showing initial application of fields, followed by a complete cycle of external fields between $\pm H_{max}=0.82H_g^*$. The arrows indicate the direction of the change of the external magnetic field. The flux profile of points A to D of the decreasing field curve will be given in Fig. 6.

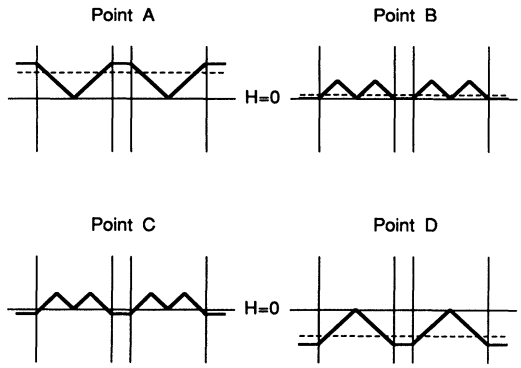

FIG. 6. The flux profiles (solid lines) of the critical state for points A, B, C, and D of the decreasing field curve in Fig. 5. Dashed lines indicate the level of the external field H_{ext}. Notice the dashed line is the *two-dimensional* average of the solid line.

$$H_m=s_p\frac{h_{f,\max}^2}{4H_g^*} \quad \text{for } h_{f,\max}<H_g^* , \tag{11a}$$

$$H_m=s_p\left[\frac{H_g^*}{2}-\frac{(h_{f,\max}-2H_g^*)^2}{4H_g^*}\right] \quad \text{for } H_g^*\le h_{f,\max}<2H_g^* , \tag{11b}$$

$$H_m=s_p\frac{H_g^*}{2} \quad \text{for } h_{f,\max}\ge 2H_g^* . \tag{11c}$$

Here $h_{f,max}$ is the value at the maximum external field H_{max}. Using Eq. (4) and the appropriate formulas in Appendix B, the exact relation between $h_{f,max}$ and H_{max} can be determined,

$$H_{\max}=s_p\frac{h_{f,\max}^2}{2H_g^*}+(1-s_p)h_{f,\max} \quad \text{for } h_{f,\max}\le H_g^* , \tag{11d}$$

$$H_{\max}=h_{f,\max}-\frac{s_pH_g^*}{2} \quad \text{for } h_{f,\max}>H_g^* . \tag{11e}$$

For a given value of H_{max}, we first solve for $h_{f,max}$ using Eqs. (11d) and (11e); then we obtain H_m using Eqs. (11a), (11b), and (11c). Further analysis of Eq. (11) indicates that H_m increases with increasing H_{max}, if $h_{f,max}$ is smaller than $2H_g^*$; and H_m becomes a constant, if $h_{f,max}$ is larger than $2H_g^*$.

IV. FLUXONS IN DISORDERED SYSTEM: HISTORY DEPENDENCES

The essence of the two-level critical state is the existence of regions where fluxons are weakly pinned and can move in and out of the sample relatively freely. These free regions cut a large sample into smaller and isolated tube-shaped (with axes in the direction of the external magnetic field) sections where fluxons are strongly pinned. The local critical state is built up in these

strong-pinned sections. For the ordered system, the size of the strong-pinned sections is equal to the grains.

Now we extend our discussion to the case of a disordered microstructure of densely packed superconducting grains. Do free regions still exist and what is the size of the strong-pinned sections? When an external magnetic field is applied to a ZFC sample, the flux will enter only the grain-boundary regions if the effective field in the grain boundaries is smaller than the lower critical field of the grains. Obviously these grain-boundary fluxons will have to bend around the grains, as shown in Fig. 7(a). As the effective field at the grain boundaries becomes larger than the lower critical field of the grains, some fluxons will enter the grains. However, if the flux-line lattice is flexible enough, which seems to be the case for the high-T_c superconductors, it is energetically more favorable for fluxons to bend around the grains and to stay in the grain-boundary regions. These fluxons are so weakly pinned that they move in and out of the sample freely, and serve the same function as the free fluxons do in the ordered system discussed in Sec. III. As shown in Fig. 7(b), which is a cross-sectional view in the direction of the external field, the sample is then divided into free regions (shown in white) and strong-pinned regions (shown in dark). Though the strong-pinned sections now are curved tubes, they are similar to the straight tubes for the ordered system in the sense that the local critical state can be built within them.

In Fig. 7(b), a fluxon in the free regions (white areas)

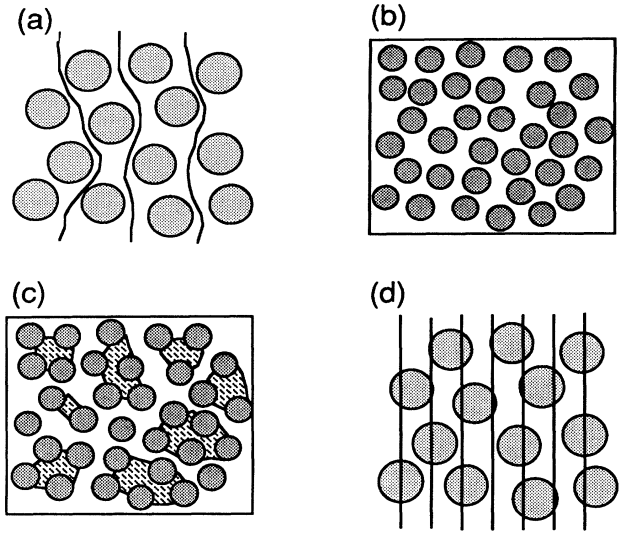

FIG. 7. A small field is applied to a ZFC sample. Fluxons go around the grains so that the structure is topologically equivalent to the ordered system. There exist distinctive free areas (in white) where fluxons are free, as well as cluster areas (in dark) where fluxon are pinned. (a) Side view for the case of a ZFC sample in a small field, where free fluxons (represented in lines) go around grains. (b) Top view of case (a). (c) Top view: For larger field, fluxons are less flexible, some free region disappears, clusters are formed. The cluster size increases as the external field increases. (d) Side view of the case of FC samples, where flux lines are straight.

can have a path through the sample (by going around the grains) without being caught by grains. Such a path would not be possible if the flux lines were straight, since a straight line passing through a densely packed random granular system is likely caught by grains and pinned strongly. Thus, as the flux lines becomes less flexible, some of the free regions as shown in Fig. 7(b) will disappear, where the flux lines cannot be bent enough to go around the grains. Correspondingly, Fig. 7(b) develops into Fig. 7(c), where in the shaded area between the grains, free fluxons no longer exist. Still, the active free or weak-pinned regions can form percolative paths, along which fluxons can move in and out of the sample freely. We may define sections (all shaded areas) enclosed by these percolative paths (white areas) as clusters. Outside the cluster, fluxons are free or weakly pinned. Within the cluster, fluxons are strongly pinned, and a local critical state exists.

In the dimension parallel to the external field, these clusters are curved tubes. Perpendicular to the external field, the cross-sectional size of the clusters is important for the local critical state. The cluster size depends on the geometry of the granular system and the flexibility of flux lines.

How to determine the cluster size L_c? One may use the elasticity theory of flux-line lattice. Since the reason for the flux line to bend around the grains is that doing so is more energetically favorable, the maximum bending is when the line tension of the curved fluxon line equals to the force preventing its entering the grains. Thus, the tilt modulus C_{44} is relevant for the discussion of the flux-line flexibility.[11] The value of C_{44} increases with increasing H, thus the flux-line lattice becomes less flexible as the external field increases. This causes the cluster size L_c to be a monotonically increasing function of $H_{\max}$, the maximum field applied to the sample. Here $H_{\max}$ is used for the following reason: When the external field is decreased from its maximum value, it is likely that the cluster size will stay about the same, for the fluxons inside the cluster will stay pinned by the grains. The lower bound of the cluster size is the grain size L_g. Therefore, we may write,

$$L_c = L_g(1+\alpha H_{\max}^{\gamma}) , \tag{12}$$

where L_g is the size of grain, $H_{\max}$ the maximum external field applied and α and γ are constants to be determined by the experimental results. The penetration field of the cluster H_c^* is

$$H_c^* \approx H_g^*(1+\alpha H_{\max}^{\gamma}) , \tag{13}$$

where H_g^* is the penetration field of the grains. Note in Eq. (13), we assume the apparent screening current in the cluster can be approximated by J_{cg}. Also, Eqs. (12) and (13) are likely to be valid for small $H_{\max}$. As $H_{\max}$ becomes larger and larger, L_c and H_c^* will saturate at the values corresponding to the FC case which we discuss later.

In order to use the result obtained in the previous section, one needs to know s_p and x, in addition to the cluster penetration field H_c^*. Equation (12) shows L_c in-

creases with the external magnetic field, but this does not necessarily mean that s_p increases with the external field because of the following reason. Due to the randomness of the granular structure, we expect that clusters with different sizes appear. For the critical-state model, larger clusters with larger H^* will contribute much more to the hysteresis curve than smaller clusters with smaller H^*. Thus one may define a characteristic cluster size L_c. Clusters significantly smaller than L_c will not contribute much to the hysteresis, and therefore, play a role similar to intergranular material. As the external field increases, grains combine to form clusters with different sizes. Since smaller clusters can be treated as though they are free regions where the critical state is concerned, it seems there is no clear definition of free regions for the critical-state model. The exact relation between s_p and the external field needs further study. In this paper, we *assume* s_p is the same as in the ordered case determined by Eq. (5),

$$s_p^{(1)} \approx s_p^{(0)} = \frac{L_g^2}{a^2} , \tag{14}$$

where we used superscript "(1)" to denote the disordered case. For the same reason, x will stay the same as determined by Eq. (7),

$$x^{(1)} \approx x^{(0)} = \frac{a - L_g}{a} . \tag{15}$$

Now, the result in Sec. III can be easily applied to the disordered system.

For the FC sample, the situation is different. The magnetic-field lines in an FC sample are straight above the transition temperature. As the sample cools down, we expect them to stay straight, as shown in Fig. 7(d). Since here the flux lines are straight, there will be very few free regions. Equation (13) is not relevant in this case, since the equivalent ZFC field would be infinitely large. The cluster size will be very large, and one expects H_c^* for the FC samples to be much larger than the one for the ZFC samples.

The above results will be compared to the experimental data in the next section, where we find that the fitting of the data on ZFC samples indeed requires that the cluster size increases with the maximum external field applied to the sample, while the data on FC samples can be fitted with a single and a much larger penetration field of the cluster.

V. MICROWAVE SURFACE RESISTANCE MEASUREMENTS OF INTERGRANULAR FLUXONS

The measurement of the microwave surface resistance enables us to study the intergranular flux motion. In this section, we report the experimental study of large two-dimensional Nb-Cu-Nb proximity-effect Josephson-junction arrays (which to some degree serve as a model system for granular superconductors) and of bulk $YBa_2Cu_3O_7$ granular superconductors, and compare the results to the model discussed in the previous sections.

Low-frequency fluxon motion in Nb-Cu-Nb proximity-effect Josephson-junction arrays has been studied recently in our laboratory, in part as a model system in the study of the granular superconductors. The fabrication process involves thermal evaporation, magnetron sputtering, rf cleaning and etching, reactive ion etching, and ultraviolet photolithography with positive and inverting photoresists. The details of the microfabrication technique have been described elsewhere.[19] A schematic top view of such an array is shown in Fig. 8. The cross-shaped niobium islands of thickness of 2000 Å are on top of a 3000 Å thick copper film. The lattice constant of the square lattice is 10 μm. Array samples with a 3/8 in. diameter circular disk geometry were fabricated on sapphire substrates. Each sample contains about 7.1×10^5 Nb islands. The normal resistance r_n is about 2 mΩ per junction. The critical current i_c is on the order of 10 μA per junction, in the temperature range of our microwave measurement. The array was placed on top of the bottom end plate of the copper microwave cavity described elsewhere.[4]

The bulk samples of $YBa_2Cu_3O_7$ are synthesized through the standard solid-state reaction method, also made in circular disk geometry of a 3/8 in. diameter, with thickness typically in the range from 1 to 2 mm. Both the dc resistivity and the surface resistance measurements show an onset transition temperature of about 92 K.[4]

The microwave system used in this experiment is described in detail in Ref. 4. We measure the reflected power from the cavity on resonance, from which we compute the sample surface resistance as follows:

$$\frac{1}{\beta} = \frac{1 \pm \sqrt{p}}{1 \mp \sqrt{p}} = \gamma_s R_s + \gamma_c R_c . \tag{16}$$

Here β is the ratio of the cavity Q to the coupling Q, $p = P_r / P_i$ is the ratio of the power reflected from the cavity at resonance to the incident power, R_s and R_c are surface resistances for the sample and the cavity, respectively, and the γ's are geometrical factors. The upper and lower signs are for the undercoupled ($\beta < 1$) and the overcoupled ($\beta > 1$) situations, respectively. At a given temperature, the surface resistance of the cavity is constant, so that $\Delta(1/\beta) \propto \Delta R_s$. Therefore, by measuring the change of $1/\beta$, we measure the change of the surface resistance of the sample, apart from a constant scale factor.

For measurements on both junction arrays and bulk $YBa_2Cu_3O_7$ samples, we used input microwave powers ranging from 1 to 10 mW. The measured $1/\beta$ are the

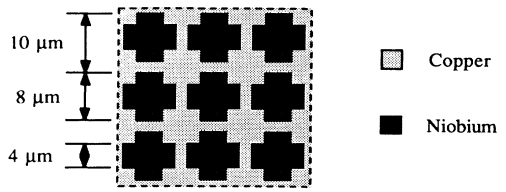

FIG. 8. Top view of a small segment of the Nb-Cu-Nb proximity Josephson-junction array sample. The cross-shaped Nb islands (shown in black) of 2000 Å thickness are on the top of a 3000 Å Cu film.

same within one percent at both power levels, indicating the currents induced by the microwave fields are much smaller than the critical currents of both arrays and bulk $YBa_2Cu_3O_7$ samples.

Though the microstructure (shown in Fig. 8) of the Nb-Cu-Nb proximity-effect Josephson-junction array is not ideal for modeling the local critical state, these arrays nevertheless provide some insight into the two-level critical-state model. Interestingly, we observe both conventional and granular behaviors in this system. The measured temperature dependence in zero field of the dc resistance and the microwave surface resistance of the Josephson-junction array shows the two-step resistive transition (e.g., Ref. 16) usually observed for the granular system. The niobium islands become superconducting at about 9 K, but thermal fluctuations prevent establishment of a coherent superconducting state through the whole sample. At the array transition temperature (i.e., the Kosterlitz-Thouless temperature) of about 4 K, a macroscopic coherent superconducting state is established as the Josephson-coupling energy overcomes the thermal fluctuations.

Figure 9(a) shows the field dependence of microwave absorption by the ZFC sample at 4.2 K. Clearly, the surface resistance in decreasing field is larger than that at the same external field during increasing fields. Also, when the field is decreased, no minimum point is reached before the field goes to zero. As discussed in Sec. I, such

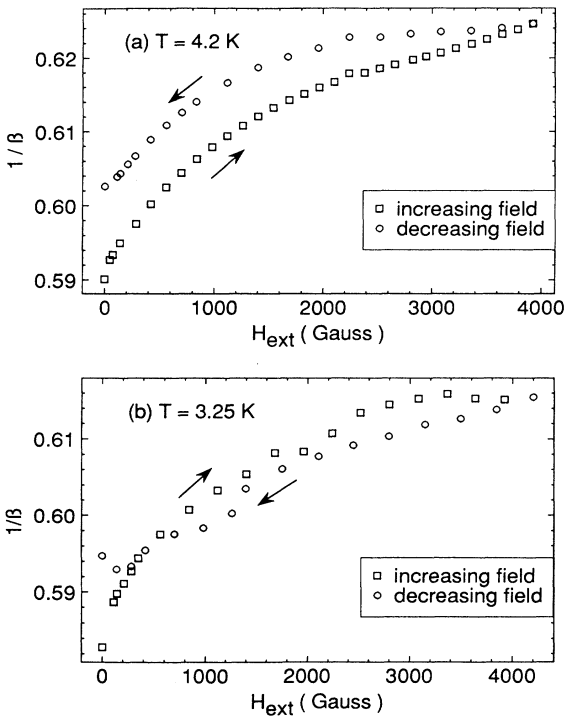

FIG. 9. (a) Surface resistance change vs external magnetic field measured on the ZFC array sample at 4.2 K (above the array transition temperature) shows the conventional behavior of Nb. (b) At 3.25 K (below the array transition temperature), it shows the behavior of a granular system. The arrows indicate the directions of the change of the external magnetic field.

behavior is expected for a classical homogeneous material. Since there is no phase coherence between the Nb islands above the array transition temperature, the intergranular contribution to the surface resistance is simply determined by the resistivity of the copper, independent of the applied field. The field-dependent change of the surface resistance should then primarily reflect the change in the *intra*granular part, i.e., the individual homogeneous Nb islands. (Because both the Nb islands and the intragranular Cu are metallic with comparable values of ρ_n, their contributions to microwave loss in these strong fields are comparable, unlike the situation of grains separated by highly resistive barriers in granular $YBa_2Cu_3O_7$.)

At temperatures below the array transition temperature, different behavior appears. Figure 9(b) shows the measurement on a ZFC sample at 3.25 K. Now the surface resistance during decreasing fields is somewhat smaller than that at the same external field during increasing fields. Also, when the field is decreased, a minimum resistance point is reached before the field goes to zero. Such behavior is consistent with our two-level model for the granular superconductors. However, it seems that the theoretical model describes the $YBa_2Cu_3O_7$ granular superconductors more quantitatively than the Josephson-junction arrays, even though the arrays have a periodic structure of the sort assumed in the ordered model. Several factors may account for this. First, each Nb island (only 3000 Å thick) is essentially a two-dimensional object perpendicular to the applied field, significantly different from our theoretical model of a three-dimensional system, where each cluster is treated as a long tube in the direction of the applied field. Second, our model [Eq. (3)] assumes the loss contribution from the grains to be negligible; this is appropriate for the discussion of granular superconductors with weakly conductive intergranular regions such as the high-T_c ceramics, but not for the Nb-Cu arrays discussed here, where both regions are metallic. A further complication in the arrays is that the strength of the superconductivity induced by the proximity effect varies continuously with position in the copper intergranular region, so that superconducting effects persist in the Cu immediately adjacent to the Nb, even when there is no effective coupling between grains. Thus, one might distinguish at least *three* distinct levels of superconductivity instead of the two on which our model is based. Accordingly, we expect at best a rough correspondence with the predictions of our model.

The typical initial and hysteresis curves of a ZFC sample of bulk $YBa_2Cu_3O_7$ have been shown in Fig. 2. It closely resembles the behavior predicted by the two-level critical-state model shown in Fig. 5. Notice that the minimum dip here is not as sharp as that shown in Fig. 5, probably due to the fact that the actual grain size is not uniform and that the critical state on the macroscopic level makes the average field vary slightly at different positions in the sample.

While the two-level critical-state model qualitatively explains our experimental results, a more quantitative agreement is difficult to achieve. Figure 10(a) shows the decreasing field curves, which are measured after various

initial maximum fields H_{max} are applied to a ZFC $YBa_2Cu_3O_7$ bulk sample at 4.2 K. Assuming the grain size of 1 μm, and a critical current density of grains to be 10^6 A/cm^2, one obtains an H_g^* of 63 G from Eq. (10). Figure 10(b) shows the calculated results based on the *ordered* system model discussed in Sec. III, with $L_g/a=0.8$, $H_g^*=100$ G. Here the positions of H_m overlap for the curves of H_{max} of 150 G or higher, as in the saturated region described by Eq. (11c), but not consistent with the experimental data shown in Fig. 10(a). Also, the ordered system model predicts that when $h_{f,max}>2H_g^*$, the decreasing field curves overlap when $0<h_f<h_{f,max}-2H_g^*$, which also disagrees with the experimental results shown in Fig. 10(a). Figure 10(c) shows the calculated results based on *disordered* system model using Eq. (12), with $L_g/a=0.8$, $H_g^*=100$ G, $\alpha^{-1}=500$ G, and the exponent γ is taken to be 1. With this model, we see that H_m changes with H_{max}, and that the curves of different H_{max} no longer overlap, which are significantly more consistent with the experimental results. Here α^{-1} is much larger than H_g^*, suggesting that the flux lines can bend around almost every grain when a field of the order of 100 G is applied to a ZFC sample. The cross section of the cluster contains only about 4 grains even at 500 G. A better fitting can be achieved by assuming a field dependent $s_p^{(1)}$ instead of a constant one used in Eq. (14), but an extra free parameter would be introduced. Moreover, for a real sample, the cluster size and the penetration field are likely to be statistically distributed, rather than a single value assumed here.

The decreasing field curve measured on the FC sample is significantly different from that of the ZFC sample. Figure 11(a) shows the decreasing field curve for the FC sample at 4.2 K cooled at various fields. Figure 11(b) is a fitting with $L_c/a=0.8$ and a single penetration field H_c^* of 1000 G [recall that Eq. (13) is not relevant in the FC case], a value corresponding to a cross section of the cluster containing about 100 grains, significantly higher than that obtained from the ZFC sample. This is in agreement with our disordered model, which predicts that the cluster size of the FC sample is much bigger, since the flux lines in the FC sample are straight. Apart from the rounding of the experimental curves caused by statistical spread of parameters, we see that the model curves in

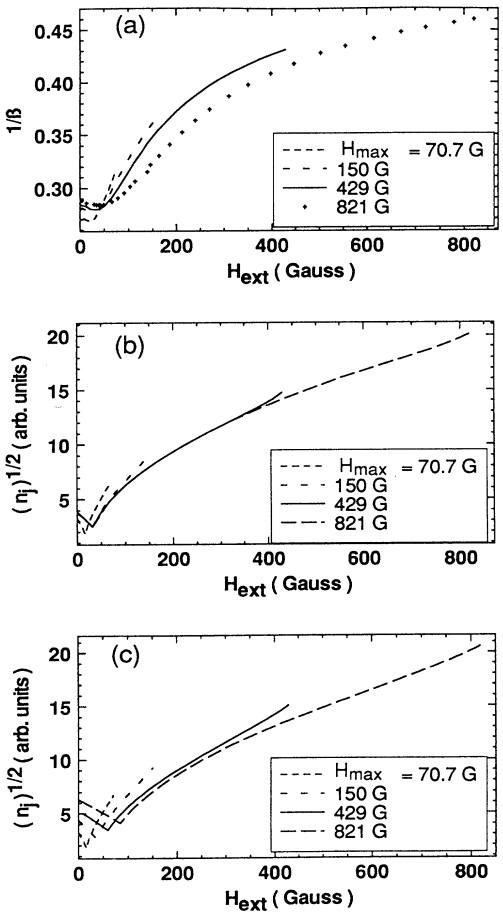

FIG. 10. (a) Decreasing-field curves of the surface resistance ($\sim 1/\beta$) hysteresis measured on a ZFC $YBa_2Cu_3O_7$ bulk sample at 4.2 K, for various maximum external fields H_{max}. (b) Calculated results based on the ordered system model described in Sec. III, with $L_g/a=0.8$ and $H_g^*=100$ G. (c) Calculated results based on the disordered system model described in Sec. IV, with $L_g/a=0.8$, $H_g^*=100$ G, and $\alpha^{-1}=500$ G; γ is taken to be 1.

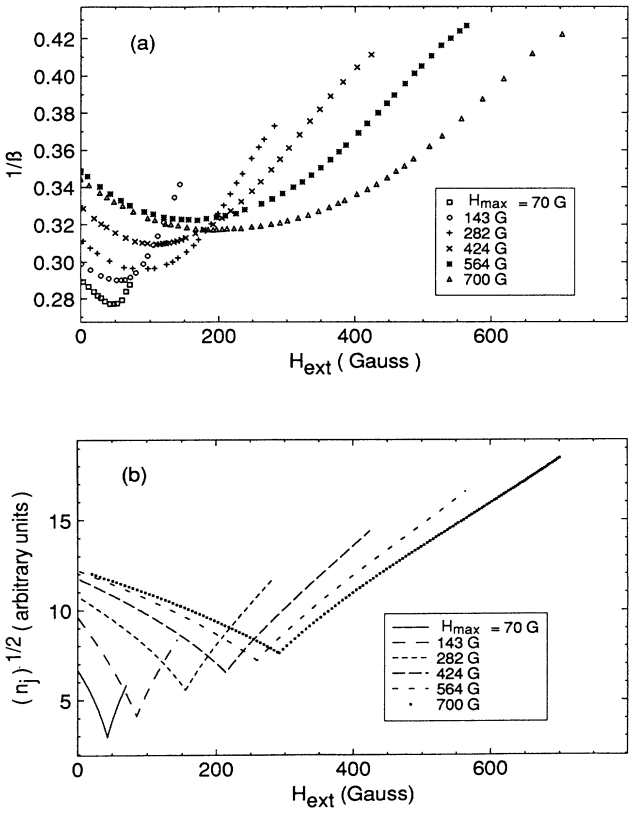

FIG. 11. (a) Decreasing-field curves of the surface resistance hysteresis measured on a FC $YBa_2Cu_3O_7$ bulk sample (same as the one in Fig. 10) at 4.2 K, for various maximum external field H_{max}. (b) Theoretical fitting with $H_c^*=1000$ G and $L_g/a=0.8$.

Fig. 11(b) capture the general features of the data quite well.

Figure 12(a) shows a different way to study the hysteresis due to intergranular fluxon motion. The surface resistance is measured when a magnetic field is first applied to a zero-field-cooled sample (shown in squares). Then the magnetic field is withdrawn, and the surface resistance is again measured (shown in circles). A change of the slopes of field dependence happens at about 40 G, corresponding to $h_{f,\max}$ passing over $2H^*$. Figure 12(b) shows the intergranular fluxon density n_j vs $H_{\rm ext}/H_g^*$ calculated for the above process using the ordered system model (Sec. III and Appendix B), where n_j becomes a constant at high field. Figure 12(c) shows the result calculated using the disordered system model (Sect. IV and Appendix B), where n_j slowly increases with $H_{\rm ext}$ at high field. The latter seems closer to the experimental case.

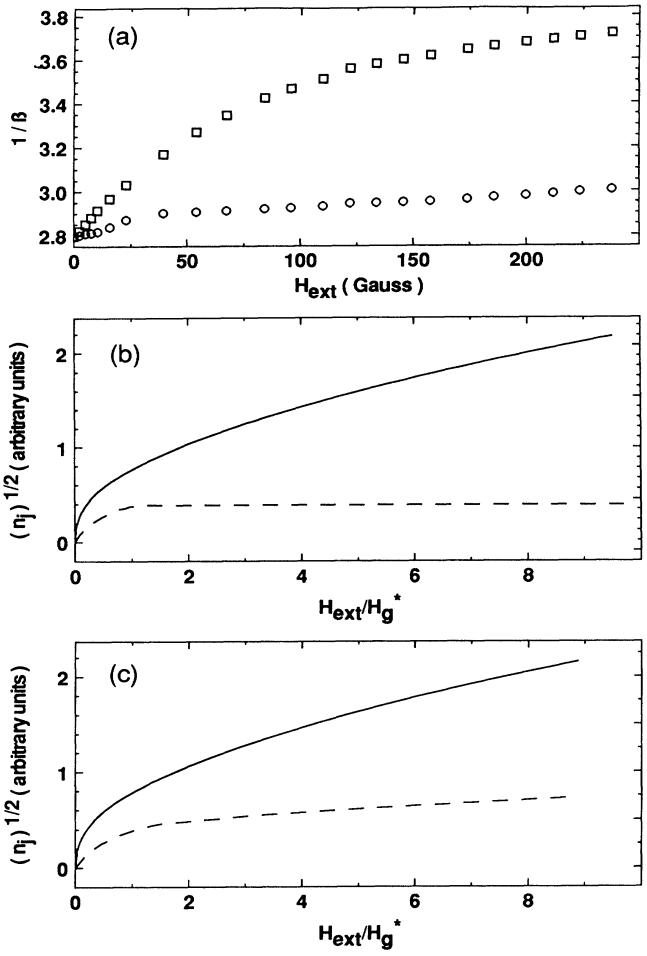

FIG. 12. (a) Squares: The surface resistance measured when the external field is first applied to a zero-field-cooled sample. Circles: The remnant surface resistance after the field is withdrawn at each $H_{\rm ext}$. The temperature is 78 K. (b) Calculated results from the ordered system model with $L_g/a=0.8$. The solid line is for a ZFC sample in an external field, and the dashed line is for the remnant surface resistance. (c) Calculated results from the disordered system model with $L_g/a=0.8$, $\alpha^{-1}=4H_g^*$, $\gamma=1$.

VI. FLUX CREEP AND TRANSPORT CRITICAL CURRENT DENSITY MEASUREMENTS

The surface resistance measurement of flux creep has been reported in a previous paper.[4] When turning off the field on either an FC or a ZFC granular sample, logarithmic decay of the surface resistance is observed. However, when a field is applied to the ZFC granular sample, a nonconventional flux creep is observed. After an initial increase over a very short time, the surface resistance *decreases* with time. Within the two-level critical-state model, this reversal in flux creep direction can be explained as follows: The *grain-boundary fluxons* that quickly enter the sample, subsequently creep into the grains, where they become immobilized and no longer contribute to the microwave loss.

Based on the ordered system model described in Sec. III and using the Bean model formulas listed in Appendix B for the local critical state in the grains, we now give a quantitative description for the time dependence of the surface resistance. The thermally activated flux creep leads to a logarithmic time dependence of the critical current, thus

$$H_g^*(t)=H_g^*(t=0)\left[1-\frac{k_BT}{U}\ln(t/\tau)\right], \tag{17}$$

where $H_g^*(t=0)$ is the value without flux creep, U is the thermal-activation energy, and τ is the characteristic time.

First, we consider the case of applying an external field $H_{\rm ext}$ to a ZFC sample, where $H_{\rm ext}$ is assumed to be larger than $2H_g^*$ for simplicity. The two-level critical state is shown in Fig. 13(a). At $H_{\rm ext}$, the value of h_f is determined by Eq. (4), and using Eq. (B2),

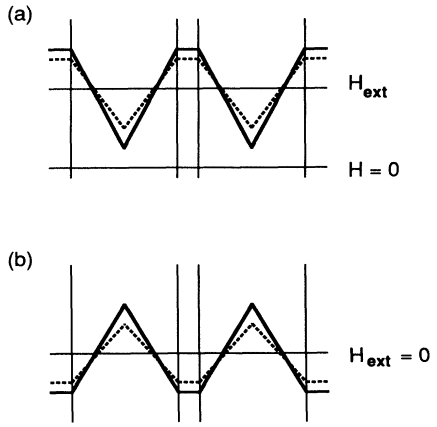

FIG. 13. Flux profiles for (a) an external field $H_{\rm ext}$ applied to the sample; (b) after the field is turned off. The solid line represents for the critical state right after the change of the field. The dashed line represents for a later time, indicating the direction of the flux creep.

$$(1-s_p)h_f+s_p\left[h_f-\frac{H_g^*(t)}{2}\right]=H_{\rm ext}\ , \tag{18}$$

which gives

$$h_f=H_{ext}+\frac{s_pH_g^*(t)}{2}\ . \tag{19}$$

Substitute Eq. (19) into Eq. (6), and using Eq. (B2) again, we have

$$\begin{aligned} n_j\Phi_0&=(1-s_p)\left[H_{\rm ext}+\frac{s_pH_g^*(t)}{2}\right]+s_px\left[H_{\rm ext}+\frac{s_pH_g^*(t)}{2}-\frac{H_g^*(t)}{2}\right] \\ &=(1-s_p+s_px)H_{\rm ext}+\left[\frac{s_p(1-s_p)(1-x)H_g^*(t=0)}{2}\right]\left[1-\frac{k_BT}{U}\ln(t/\tau)\right]\ . \end{aligned} \tag{20}$$

Note that in Eq. (20), the first bracket in the second term is always positive, since s_p and x are always smaller than unity; thus n_j will *decrease* logarithmically with time.

Secondly, we consider the case that the external field $H_{\rm ext}$ applied to and then withdrawn from a ZFC sample or that the field is withdrawn from a FC sample cooled in $H_{\rm ext}$. Again, $H_{\rm ext}$ is assumed to be larger than $2H_g^*$ for simplicity. When the field is withdrawn, the two-level critical state is shown in Fig. 13(b), which is independent of the previously applied field $H_{\rm ext}$. At $H_{\rm ext}=0$, the value of h_f is determined by Eq. (4), and using Eq. (B9),

$$(1-s_g)h_f+s_g\left[h_f+\frac{H_g^*(t)}{2}\right]=0\ , \tag{21}$$

which gives

$$h_f=-\frac{s_gH_g^*(t)}{2}\ . \tag{22}$$

Substitute Eq. (22) into Eq. (6), and using Eqs. (B9) and (B11), we have

$$\begin{aligned} n_j\Phi_0&=(1-s_g)\left|-\frac{s_gH_g^*(t)}{2}\right|+s_gx\left[-\frac{s_gH_g^*(t)}{2}+\frac{H_g^*(t)}{2}+\frac{(s_gH_g^*(t)/2)^2}{2H_g^*(t)}\right] \\ &=\left[s_g(1-s_g)(1+x)+\frac{xs_g^3}{4}\right]\left[\frac{H_g^*(t=0)}{2}\right]\left[1-\frac{k_BT}{U}\ln(t/\tau)\right]\ . \end{aligned} \tag{23}$$

Equation (23) shows that n_j will again *decrease* logarithmically with time.

In summary, whether an external field is applied to a granular sample, or the previously applied field is withdrawn from the sample, the surface resistance will decrease with time for both cases. Figure 14 shows the experimental results for both cases. In the case that an external field is applied to the sample as shown in Fig. 14(a), the surface resistance initially increases with time since, at the macroscopic level, the flux creeps into the sample and increases the surface resistance. At a later time, the process of the *grain-boundary fluxons* creeping into the less-dissipative grains becomes dominant, and the surface resistance decreases with time as predicted by Eq. (23). The data in Fig. 14(b) show a much cleaner logarithmically decay measured after the field is withdrawn; it gives a value of the activation energy at 78 K of about 0.1 eV.

The motion of fluxons determines many other properties such as the critical current density. For a conventional homogeneous superconductor, fluxons are trapped by pinning sites in the sample as the field is decreased, and the maximum value of J_c can only be reached at a negative external field where the total number of fluxons is a minimum. However, the macroscopic critical current density J_c in the granular superconductor is greatly influenced by the intergranular flux density instead of the total flux density in the sample, and thus, the field dependence of J_c should be similar to our microwave study result. Several groups have studied some anomalous magnetic-field dependences of the transport critical current density J_c measured on bulk polycrystalline $YBa_2Cu_3O_7$.[20–22] When a magnetic field is applied to a ZFC sample and then slowly reduced, J_c increases and reaches a maximum value before the external field reaches zero. Evetts and Glowacki qualitatively analyzed their data with a simple model consisting of two grains and one grain boundary.[20] They proposed that the anomalous maximum of the critical current density in the granular samples is due to the fact that the flux trapped in the grains provides a field opposite to the external field in the grain boundary and therefore, zero flux in the grain boundaries can be reached when the external field is still positive. Such a picture is similar to the conclusions drawn from the more detailed two-level critical-state model proposed here. However, they did not analyze their data analytically, since the shapes of their hysteresis curves depend on the critical current density criteria be-

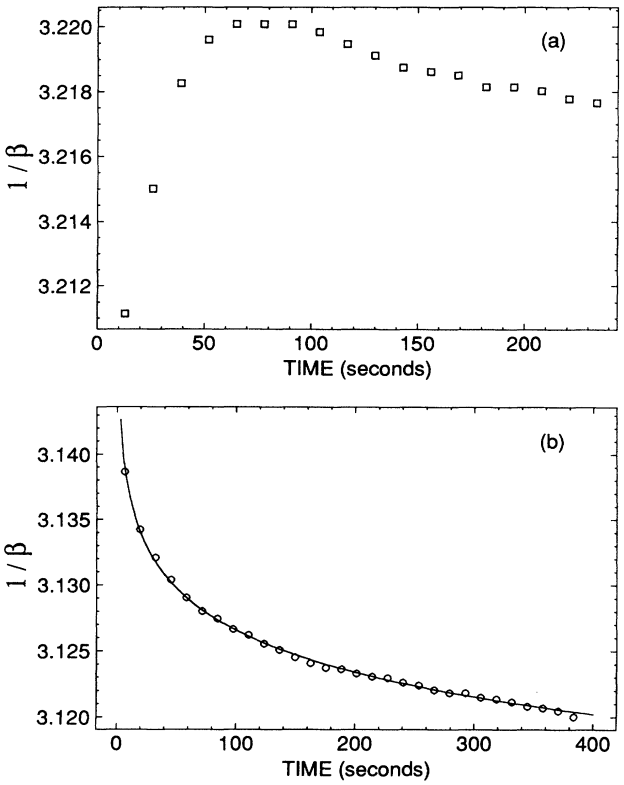

FIG. 14. Time dependence of the surface resistance measured on a $YBa_2Cu_3O_7$ ceramic sample at 78 K. (a) An external magnetic field of 65 G is applied to a ZFC sample at $t=0$. (b) A previously applied field of 65 G is turned off at $t=0$. The line represents a logarithmic fitting with a thermal activation energy $U=0.1$ eV.

ing used. Our microwave data shows no power dependence, presumably because, within our power range, the perturbational rf currents induced in the sample are much smaller than the critical current density of the sample.

The magnetization data should show the granularity-related effects, even if it is the total flux density that is measured, because the intergranular current can influence the change of total flux density. However, the situation there is more complicated and the assumptions made in our calculation for the intergranular fluxon density are no longer useful (for example, for an infinitely large flat slab, the total magnetization is zero).

VII. CONCLUSION

In conclusion, the proposed two-level critical-state model deals with the flux profiles on both macroscopic and local levels. While the exact solution for an arbitrary sample geometry requires numerical calculation, we can solve a special case of an infinitely large flat slab in a perpendicular magnetic field. The model reveals anomalous behavior that is unexpected from the single level critical-state model used for homogeneous superconductors. Our measurements of the magnetic-field hysteresis of the microwave surface resistance of bulk samples of $YBa_2Cu_3O_7$ and of the Nb-Cu-Nb proximity-effect Josephson-junction arrays are in reasonable agreement with the two-level model, though more quantitative work is needed to understand the clusters we described in Sec. IV. Our study has shown that the microwave surface resistance measurement provides a unique tool for the study of the intergranular fluxons.

ACKNOWLEDGMENTS

We are pleased to acknowledge useful discussions with Professor C. J. Lobb. We would also like to thank Dr. S. P. Benz for his development of the array fabrication procedure. This work was suppported in part by National Science Foundation (NSF) Grants No. DMR-89-20490 and DMR-89-12927, and by ONR Grants No. N00014-89-J-1565 and N00014-89-J-1023.

APPENDIX A: KIM-ANDERSON MODEL FOR A LONG SLAB OF PENETRATION FIELD H^*

Here we give the formulas we used for the Kim-Anderson model,[10] where $J_c=\alpha/h$. The penetration field H^* in a parallel field is related to the thickness of the slab D,

$$H^*=\sqrt{4\pi\alpha D}\ .$$

The following formulas for the initial and the hysteresis curves are calculated according to the critical-state model, for the case that the maximum external field is smaller than H^*. The formulas for $\langle h\rangle$ were previously calculated in Ref. 13, where $\langle h\rangle$ was denoted as B. (I) Initial application of field H to a ZFC sample, where H is smaller than H^*:

$$\langle h\rangle=\langle|h|\rangle=\frac{2H^3}{3H^{*2}} \quad \text{for } H\le H^*\ . \tag{A1}$$

(II) Hysteresis curves for a ZFC sample, where H is cycled between $\pm H_0$, and $H_0<H^*$:

$$\langle h\rangle=\pm\left[\frac{2H_0^3}{3H^{*2}}\right]\times\left\{\frac{1}{\sqrt{2}}\left[\left[1\pm\frac{H}{H_0}\left|\frac{H}{H_0}\right|\right]\right]^{3/2}-\left|\frac{H}{H_0}\right|^3\right\}, \tag{A2}$$

where + and − signs apply for increasing and decreasing fields, respectively. For decreasing field,

$$\langle|h|\rangle=\langle h\rangle \quad \text{for } H_0>H>0\ , \tag{A3}$$

$$\langle|h|\rangle=\langle h\rangle+\frac{3H^3}{2H^{*2}} \quad \text{for } 0>H>-H_0\ . \tag{A4}$$

For increasing field,

$$\langle|h|\rangle=-\langle h\rangle \quad \text{for } -H_0<H<0\ , \tag{A5}$$

$$\langle|h|\rangle=-\langle h\rangle+\frac{3H^3}{2H^{*2}} \quad \text{for } 0<H<H_0\ , \tag{A6}$$

where $\langle h\rangle$ is given in Eq. (A2).

APPENDIX B: BEAN MODEL FOR A LONG SLAB OF PENETRATION FIELD H^*

In this section, we give the results of calculations of $\langle h_p \rangle$ and $\langle |h_p| \rangle$ for a long slab in a parallel field, with h_p to denote the flux density in the slab and h_f to denote the parallel external field. A constant critical current density is assumed, as usual with the Bean model, and the penetration field H^* is related to the slab thickness D,

$$H^* \approx \frac{2\pi}{c} J_c D \ .$$

Again, some of the following formulas were previously calculated in Ref. 13. (I) Initial application of field to a ZFC sample

$$\langle h_p \rangle = \langle |h_p| \rangle = \frac{h_f^2}{2H^*} \quad \text{for } h_f \le H^* \ , \tag{B1}$$

$$\langle h_p \rangle = \langle |h_p| \rangle = h_f - \frac{H^*}{2} \quad \text{for } h_f \ge H^* \ . \tag{B2}$$

(II) Hysteresis curves for a ZFC sample, where h_f is cycled between $\pm h_0$: (1) If $h_0 \le H^*$,

$$\langle h_p \rangle = \frac{h_f h_0}{2H^*} \pm \frac{h_f^2 - h_0^2}{4H^*} \ , \tag{B3}$$

where + and − signs apply for increasing and decreasing fields, respectively. For decreasing field,

$$\langle |h_p| \rangle = \langle h_p \rangle \quad \text{for } h_0 > h_f > 0 \ , \tag{B4}$$

$$\langle |h_p| \rangle = \langle h_p \rangle + \frac{h_f^2}{H^*} \quad \text{for } 0 > h_f > -h_0 \ . \tag{B5}$$

For increasing field,

$$\langle |h_p| \rangle = -\langle h_p \rangle \quad \text{for } -h_0 < h_f < 0 \ , \tag{B6}$$

$$\langle |h_p| \rangle = -\langle h_p \rangle + \frac{h_f^2}{H^*} \quad \text{for } 0 < h_f < h_0 \ . \tag{B7}$$

(2) If $h_0 \ge H^*$, for decreasing field,

$$\langle h_p \rangle = h_f + \frac{H^*}{2} - \frac{(h_f - h_0 + 2H^*)^2}{4H^*} \quad \text{for } h_0 > h_f > h_0 - 2H^* \ , \tag{B8}$$

$$\langle h_p \rangle = h_f + \frac{H^*}{2} \quad \text{for } h_0 - 2H^* > h_f > -h_0 \ , \tag{B9}$$

$$\langle |h_p| \rangle = \langle h_p \rangle \quad \text{for } h_0 > h_f > 0 \ , \tag{B10}$$

$$\langle |h_p| \rangle = \langle h_p \rangle + \frac{h_f^2}{H^*} \quad \text{for } 0 > h_f > -H^* \ , \tag{B11}$$

$$\langle |h_p| \rangle = -\langle h_p \rangle \quad \text{for } -H^* > h_f > -h_0 \ . \tag{B12}$$

For increasing field,

$$\langle h_p \rangle = h_f - \frac{H^*}{2} + \frac{(h_f + h_0 - 2H^*)^2}{4H^*} \quad \text{for } -h_0 < h_f < -h_0 + 2H^* \ , \tag{B13}$$

$$\langle h_p \rangle = h_f = \frac{H^*}{2} \quad \text{for } -h_0 + 2H^* < h_f < h_0 \ , \tag{B14}$$

$$\langle |h_p| \rangle = -\langle h_p \rangle \quad \text{for } -h_0 < h_f < 0 \ , \tag{B15}$$

$$\langle |h_p| \rangle = -\langle h_p \rangle + \frac{h_f^2}{H^*} \quad \text{for } 0 < h_f < H^* \ , \tag{B16}$$

$$\langle |h_p| \rangle = \langle h_p \rangle \quad \text{for } H^* < h_f < h_0 \ . \tag{B17}$$

(III) For a FC sample (cooled in a field of h_0). For decreasing external field, h_0 is decreasing,

$$\langle h_p \rangle = h_0 - \frac{(h_f - h_0)^2}{2H^*} \quad \text{for } h_0 > h_f > h_0 - H^* \ , \tag{B18}$$

$$\langle h_p \rangle = h_f + \frac{H^*}{2} \quad \text{for } h_0 - H^* > h_f \ , \tag{B19}$$

$$\langle |h_p| \rangle = \langle h_p \rangle \quad \text{for } h_0 > h_f > 0 \ , \tag{B20}$$

$$\langle |h_p| \rangle = \langle h_p \rangle + \frac{h_f^2}{H^*} \quad \text{for } 0 > h_f > -H^* \ , \tag{B21}$$

$$\langle |h_p| \rangle = -\langle h_p \rangle \quad \text{for } -H^* > h_f . \tag{B22}$$

*Present address: Department of Physics, State University of New York at Stony Brook, Stony Brook, NY 11794.

[1] A. M. Portis, K. R. Blazey, K. A. Müller, and J. G. Bednorz, Europhys. Lett. **5**, 467 (1988).
[2] E. J. Pakulis and T. Osada, Phys. Rev. B **37**, 5940 (1988).
[3] Q. Li, K. W. Rigby, and M. S. Rzchowski, Phys. Rev. B **39**, 6607 (1989).
[4] L. Ji, M. S. Rzchowski, and M. Tinkham, Phys. Rev. B **42**, 4838 (1990).
[5] A. Gould, S. M. Bhagat, M. A. Manheimer, and S. Tyagi, J. Appl. Phys. **67**, 5020 (1990); A. Gould, M. Huang, S. M. Bhagat, and S. Tyagi, *ibid.* **69**, 4880 (1991).
[6] L. Ji, Ph.D. thesis, Harvard University, 1991; L. Ji, M. S. Rzchowski, N. Anand, and M. Tinkham, Bull. Am. Phys. Soc. **36**, 666 (1991).
[7] J. I. Gittleman and B. Rosenblum, Phys. Rev. Lett. **16**, 734 (1966); J. I. Gittleman and B. Rosenblum, J. Appl. Phys. **39**, 2617 (1968).
[8] J. Bardeen and M. J. Stephen, Phys. Rev. **140**, A1197 (1965); M. J. Stephen and J. Bardeen, Phys. Rev. Lett. **14**, 112 (1965).
[9] C. P. Bean, Phys. Rev. Lett. **8**, 250 (1962); C. P. Bean, Rev. Mod. Phys. **36**, 31 (1964).
[10] Y. B. Kim, C. F. Hempstead, and A. R. Strnad, Phys. Rev. **129**, 528 (1963); P. W. Anderson and Y. B. Kim, Rev. Mod. Phys. **36**, 39 (1964).
[11] A. M. Campell and J. E. Evetts, Adv. Phys. **21**, 199 (1972).
[12] D.-X. Chen and R. B. Goldfarb, J. Appl. Phys. **66**, 2489 (1989).
[13] L. Ji, R. H. Sohn, G. C. Spalding, C. J. Lobb, and M. Tinkham, Phys. Rev. B **40**, 10 936 (1989).

[14]A. M. Portis and K. W. Blazey, Solid State Commun. **68**, 1097 (1988).
[15]John R. Clem, Physica C **153-155**, 50 (1988).
[16]M. Tinkham and C. J. Lobb, *Solid State Physics* (Academic, San Diego, 1989), Vol. **42**, pp. 91–134.
[17]A. Gurevich, Phys. Rev. B **42**, 4857 (1990).
[18]J. H. Van Vleck, *Theory of Electric and Magnetic Susceptibilities* (Oxford University Press, London, 1932).
[19]M. S. Rzchowski, S. P. Benz, M. Tinkham, and C. J. Lobb, Phys. Rev. B **42**, 2041 (1990); S. P. Benz, M. S. Rzchowski, M. Tinkham, and C. J. Lobb, *ibid.* **42**, 6165 (1990).
[20]J. E. Evetts and B. A. Glowacki, Cryogenics **28**, 641 (1988).
[21]M. E. McHenry, M. P. Maley, and J. O. Willis, Phys. Rev. B **40**, 2666 (1989).
[22]D. Dimos, P. Chaudhari, and J. Mannhart, Phys. Rev. B **41**, 4038 (1990).